EUROPEAN ORGANIZATION FOR NUCLEAR RESEARCH

CERN-EP-2021-090
12 May 2021

Search for lepton number and flavour violation in K^+ and π^0 decays

The NA62 Collaboration[1]

[1] *Authors are listed at the end of this Letter.*

Searches for the lepton number violating $K^+ \to \pi^-\mu^+e^+$ decay and the lepton flavour violating $K^+ \to \pi^+\mu^-e^+$ and $\pi^0 \to \mu^-e^+$ decays are reported using data collected by the NA62 experiment at CERN in 2017–2018. No evidence for these decays is found and upper limits of the branching ratios are obtained at 90% confidence level: $\mathcal{B}(K^+ \to \pi^-\mu^+e^+) < 4.2\times10^{-11}$, $\mathcal{B}(K^+ \to \pi^+\mu^-e^+) < 6.6 \times 10^{-11}$ and $\mathcal{B}(\pi^0 \to \mu^-e^+) < 3.2 \times 10^{-10}$. These results improve by one order of magnitude over previous results for these decay modes.

I. INTRODUCTION

Discovery of Lepton Number (LN) or Lepton Flavour number (LF) violation would be a clear indication of new physics; although they are conserved quantum numbers in the Standard Model (SM), their conservation is not imposed by any local gauge symmetry. Observation of neutrino oscillations provided the first proof of the non-conservation of LF, however no evidence of LN violation has been observed so far. New physics models which explain experimental observations, such as neutrino oscillations or the possible flavour anomalies in B-physics [1], can introduce LN and LF violation. The see-saw mechanism [2] provides a source of LN violation through the exchange of Majorana neutrinos, as in neutrinoless double beta decay. Processes violating LF conservation can occur via the exchange of leptoquarks [3, 4], of a Z' boson [5, 6] or in SM extensions with light pseudoscalar bosons [7]. Searches for kaon decays violating LN and LF conservation are powerful probes of models beyond the SM at mass scales up to $\mathcal{O}(100\,\text{TeV})$. These complement searches in B meson or lepton decays, such as those producing recent limits on branching ratios $\mathcal{B}(B^+ \to K^+\mu^-e^+) < 7.0 \times 10^{-9}$ [8] and $\mathcal{B}(\mu^+ \to e^+\gamma) < 4.2 \times 10^{-13}$ [9], which explore different aspects of new physics models. An indirect upper limit on $\mathcal{B}(K^+ \to \pi^-\mu^+e^+)$ of a few units $\times10^{-11}$ has been derived from an upper limit on the $\mu^- + (Z, A) \to e^+ + (Z-2, A)$ conversion probability [10]. Previous experimental limits on LN and LF violating K^+ and π^0 decays are reported in Table I.

In this letter searches are presented for the LN violating $K^+ \to \pi^-\mu^+e^+$ decay (π^- channel), and the LF violating decays $K^+ \to \pi^+\mu^-e^+$ (μ^- channel) and $\pi^0 \to \mu^-e^+$, using the data collected by the NA62 experiment at the CERN SPS in 2017–2018.

TABLE I: Summary of previous experimental limits at 90% CL on the branching ratios of LN and LF violating K^+ and π^0 decays.

	Limit at 90% CL
$K^+ \to \pi^-\mu^+\mu^+$	$< 4.2 \times 10^{-11}$ (NA62 at CERN [11])
$K^+ \to \pi^-e^+e^+$	$< 2.2 \times 10^{-10}$ (NA62 at CERN [11])
$K^+ \to \pi^-\mu^+e^+$	$< 5.0 \times 10^{-10}$ (E865 at BNL [12])
$K^+ \to \pi^+\mu^-e^+$	$< 5.2 \times 10^{-10}$ (E865 at BNL [12])
$K^+ \to \pi^+\mu^+e^-$	$< 1.3 \times 10^{-11}$ (E865 at BNL [13])
$\pi^0 \to \mu^-e^+$	$< 3.4 \times 10^{-9}$ (E865 at BNL [12])
$\pi^0 \to \mu^+e^-$	$< 3.8 \times 10^{-10}$ (E865 at BNL [14])
$\pi^0 \to \mu^\pm e^\mp$	$< 3.6 \times 10^{-10}$ (KTeV at FNAL [15])

II. BEAMLINE AND DETECTOR

A sketch of the NA62 beamline and detector is shown in Figure 1 and a detailed description can be found in [16]. Kaons are produced in the interaction of a high intensity 400 GeV proton beam extracted from the CERN SPS with a beryllium target. The resulting secondary hadron beam of positively charged particles consists of 70% π^+, 23% protons, and 6% K^+, with a nominal momentum of 75 GeV/c (1% rms momentum bite). Beam kaons are identified by a differential Cherenkov counter (KTAG) with 70 ps time resolution and reconstructed using a silicon pixel beam spectrometer (GTK). The momenta and directions of charged particles produced in K^+ decays in a 75 m long fiducial volume (FV) are measured by a magnetic spec-

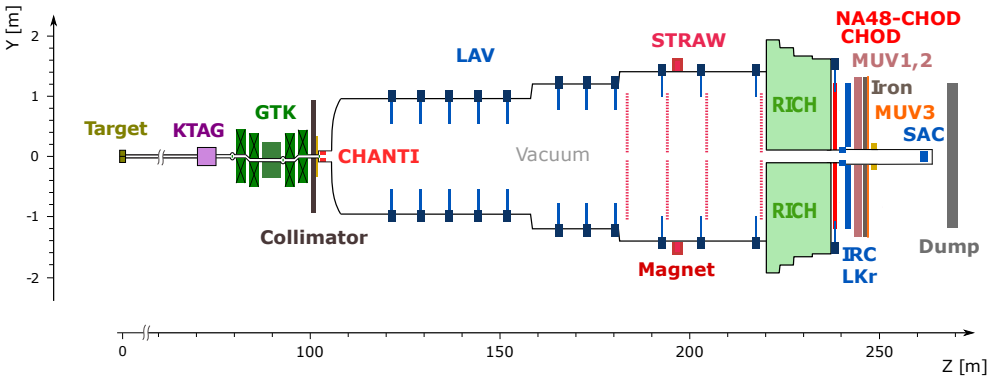

FIG. 1: Schematic side view of the NA62 beamline and detector. Information from the CHANTI, IRC and SAC veto detectors, MUV1,2 hadronic calorimeters, and GTK beam spectrometer is not used in this analysis.

trometer (STRAW). Particle identification is provided by a ring-imaging Cherenkov detector (RICH), a quasi-homogeneous liquid krypton electromagnetic calorimeter (LKr), hadronic calorimeters (MUV1,2) and a muon detector (MUV3). A photon veto system includes the LKr, twelve ring-shaped lead-glass detectors (LAV1–12) and small angle calorimeters (IRC and SAC). The RICH provides a trigger time with 70 ps precision. Two scintillator hodoscopes, NA48-CHOD and CHOD, each arranged in four quadrants, provide trigger signals and time measurements for charged particles with 200 ps and 800 ps precision, respectively.

III. DATA SAMPLE AND TRIGGER

The data sample consists of 8.3×10^5 SPS spills collected in 2017 and 2018 with a typical primary beam intensity of 2.2×10^{12} protons per spill of three seconds effective duration, corresponding to a mean K^+ decay rate in the FV of 3.7 MHz. The trigger system is composed of a hardware level (L0) and a software level (L1), with maximum output rates of 1 MHz and 10 kHz, respectively [17]. The three trigger chains used for this analysis run concurrently with the trigger chain dedicated to the main goal of the experiment, the measurement of the $K^+ \to \pi^+ \nu\bar{\nu}$ branching ratio [18]: the multi-track (MT), electron multi-track (eMT), and muon multi-track (μMT) triggers.

The MT L0 trigger requires a signal in the RICH, and a time coincidence of signals in two opposite CHOD quadrants. The eMT trigger collects a sample enriched with electrons, which deposit almost all of their energy in the LKr, by additionally requiring a minimum energy deposit of 20 GeV in the LKr (LKr20 signal). The μMT trigger selects at least one muon in the final state, requiring in addition to the MT conditions a coincident signal in the MUV3 and a minimum energy deposit of 10 GeV in the LKr (LKr10 signal). The common L1 trigger conditions select events with a K^+ identified by the KTAG within 5 ns of the trigger time, and a track of a negatively charged particle reconstructed in the STRAW. For most of the data sample the L1 μMT trigger also requires fewer than 3 signals in total in LAV stations 2–11 within 6 ns of the trigger time. The MT, μMT, and eMT trigger chains are downscaled typically by factors $D_{\rm MT} = 100$, $D_{\mu{\rm MT}} = 8$, and $D_{e{\rm MT}} = 8$, respectively, but these values were varied during data-taking.

Data collected with a minimum bias trigger, requiring the presence of a signal in the NA48-CHOD at L0 and downscaled by a factor of 400, are used for particle identification and trigger efficiency studies.

IV. ANALYSIS STRATEGY AND EVENT SELECTION

The branching ratios for signal decays are measured relative to the normalisation channel $K^+ \to \pi^+\pi^+\pi^-$ ($K_{3\pi}$) which, because of a similar topology to the signal decays, allows a first order cancellation of systematic effects related to trigger conditions and detector inefficiencies.

The MT, eMT, and μMT trigger chains are used to collect signal events, and the MT trigger chain is used to collect normalisation events.

Acceptances for the signal and normalisation channels are evaluated using Monte Carlo (MC) detector simulations based on the GEANT4 toolkit [19].

The event selection identifies events comprising three tracks which point to the active region of the downstream detectors used in the analysis, are within 5 ns of the trigger time, and form a vertex of total charge +1 with a longitudinal distance from the target $105 < Z_{vtx} < 180$ m. A vertex time is defined as the weighted mean of the track times, with weights assigned based on the time resolution of the detector (CHOD or NA48-CHOD) used to define the track time. To confirm that the beam particle is a K^+, a KTAG signal must be present within 3 ns of the vertex time. Events with LAV signals within 3 ns of the trigger time are rejected, providing a photon veto. The total three-momentum at the vertex must have a magni-

tude consistent with the measured mean K^+ beam momentum within 2.5 GeV/c and its transverse component with respect to the beam axis is required to be less than 35 MeV/c, to reject events with missing energy.

For the normalisation channel selection, the three-track invariant mass reconstructed under the 3π mass hypothesis is required to be consistent with the charged kaon mass within $3\sigma_{3\pi}$, where the measured mass resolution is $\sigma_{3\pi} = 0.9$ MeV/c^2.

Signal selection requires particle identification (PID) conditions using information from the LKr and MUV3 detectors to isolate candidate $\pi^\mp\mu^\pm e^+$ final states. For each track the ratio, E/p, is calculated from the energy (E) of the associated LKr cluster and its momentum (p). If no signal in MUV3 is associated with the track, a pion is identified if $E/p < 0.9$ while a positron is identified if $0.95 < E/p < 1.05$. For a positron, exactly one associated LKr cluster must be found. A muon is identified if a MUV3 signal is associated with the track and $E/p < 0.2$. The range of the vertex longitudinal position is optimised to reduce the background from K^+ decays upstream of the FV. It is required that $Z_{vtx} > 107\,(111)$ m for the π^- (μ^-) channel.

For the π^- channel selection, the mass of the π^-e^+ pair calculated under the e^-e^+ mass hypothesis is required to exceed 140 MeV/c^2. This condition rejects backgrounds from $K^+ \to \pi^+\pi^0$ and $K^+ \to \pi^0\ell^+\nu_\ell$ ($\ell = \mu, e$) decays followed by $\pi^0 \to e^+e^-\gamma$, with an e^- misidentified as a π^-.

The kinematic variable used to distinguish between signal and background is the invariant mass of the three charged tracks, $m_{\pi\mu e}$, computed by assigning the π, μ, e mass hypotheses to the tracks with corresponding identities defined by the PID requirements. The $m_{\pi\mu e}$ region close to the charged kaon mass, m_K [20], 478–510 MeV/c^2 is kept masked to avoid bias in the selection optimisation. This includes the signal region, 490–498 MeV/c^2, and 12 MeV/c^2 wide control regions immediately below and above the signal region (denoted CR1 and CR2 respectively), used at the final stage of the analysis to validate the background prediction. The $m_{\pi\mu e}$ resolution, obtained from simulation, is 1.4 MeV/c^2.

The search for the decay chain $K^+ \to \pi^+\pi^0$ followed by $\pi^0 \to \mu^-e^+$, is performed on the sample of events passing the μ^- channel selection by requiring that the reconstructed mass of the μe pair is consistent with the π^0 mass, $|m_{\mu e} - m_{\pi^0}| < 2$ MeV/c^2. The $m_{\mu e}$ resolution obtained from simulation is 0.4 MeV/c^2.

V. TRIGGER EFFICIENCY

The trigger efficiency is measured with minimum bias data. For the abundant normalisation $K_{3\pi}$ events the efficiency is measured directly. On the other hand, for the signal an enriched signal-like sample is used which is selected by loosening requirements on Z_{vtx} and requiring that $m_{\pi\mu e}$ is outside the masked region. The measured

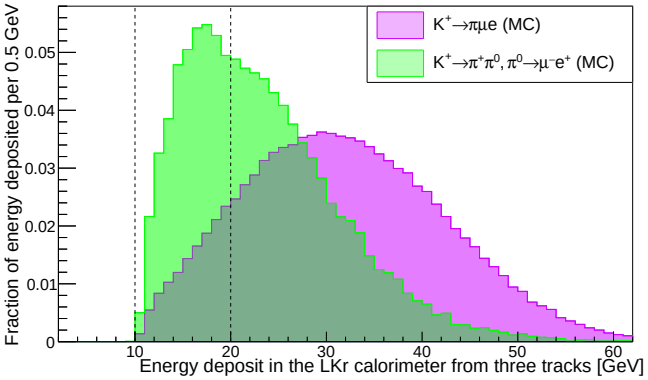

FIG. 2: Distributions of energy deposited in the LKr associated with the three selected STRAW tracks for events passing the signal selection, $K^+ \to \pi^\pm\mu^\mp e^+$ and $K^+ \to \pi^+\pi^0$ followed by $\pi^0 \to \mu^-e^+$, obtained from MC simulations after data-driven corrections to the energy of the LKr pion cluster.

efficiency of the MT trigger for normalisation events is $\varepsilon_{\rm n} = (93.2 \pm 0.5) \times 10^{-2}$, and the result for signal-like events is consistent with $\varepsilon_{\rm n}$ within 1%. The main source of MT trigger inefficiency is the STRAW condition at L1, and the uncertainty accounts for variations in the measured efficiency over time.

The L0 MUV3 and L1 LAV conditions in the μMT trigger have negligible inefficiency for signal-like events since similar conditions are applied offline in the selection. The efficiencies of the LKr10 and LKr20 conditions present in the μMT and eMT triggers, respectively, depend on the total energy deposited in the LKr. The energy deposited by the pion in the LKr is not precisely reproduced in simulations, so a correction to this quantity is applied based on measurements. After this correction, energy-dependent trigger inefficiencies are applied in the simulation. The softer electron spectrum for $K^+ \to \pi^+\pi^0$ followed by $\pi^0 \to \mu^-e^+$ decays, with respect to $K^+ \to \pi^\pm\mu^\mp e^+$ (Figure 2), leads to a lower efficiency of the LKr10 and LKr20 trigger conditions, as will be shown below.

VI. NORMALISATION TO $K_{3\pi}$ DECAY

The effective number of K^+ decays in the FV is

$$N_K = \sum_i N_K^i = \frac{1}{\mathcal{B}(K_{3\pi})A_{\rm n}\varepsilon_{\rm n}} \cdot \sum_i \left(N_{3\pi}^i \frac{D_{\rm MT}^i}{D_{\rm eff}^i} \right) = (1.33 \pm 0.02) \times 10^{12}\,, \quad (1)$$

where the index i runs over data-taking periods defined by constant trigger downscaling factors, $N_{3\pi}^i$ are the numbers of normalisation $K_{3\pi}$ events selected with the MT trigger with downscaling factor $D_{\rm MT}^i$, and $D_{\rm eff}^i$ are the effective downscaling factors of the three signal trig-

ger chains. These are evaluated as

$$D^i_{\rm eff} = \left[1-\left(1-\frac{1}{D^i_{\rm MT}}\right)\left(1-\frac{1}{D^i_{\mu{\rm MT}}}\right)\left(1-\frac{1}{D^i_{e{\rm MT}}}\right)\right]^{-1} \quad (2)$$

and vary in the range 3.2–6.9. In Eq. (1), $\mathcal{B}(K_{3\pi}) = (5.583\pm0.024)\times10^{-2}$ [20] and $A_{\rm n} = 10.18\times10^{-2}$ are the branching ratio and selection acceptance (determined using simulation) of the $K_{3\pi}$ decay, and $\varepsilon_{\rm n}$ is the efficiency of the MT trigger for the normalisation channel. The total number of selected $K_{3\pi}$ events collected with the MT trigger is $\sum_i N^i_{3\pi} = 2.73\times10^8$. The quoted uncertainty in N_K accounts for any inaccuracy in the description of the beam momentum spectrum and STRAW inefficiency in simulations.

VII. BACKGROUNDS

Backgrounds arise from K^+ decays followed by particle misidentification and $\pi^\pm \to \ell^\pm\nu_\ell$ ($\ell = \mu, e$) decays in flight. The probability of at least one $\pi^\pm$, from a $K_{3\pi}$ decay in the FV, to decay upstream of the LKr is found using simulations to be 7.5%, with the ratio of decay rates $\Gamma(\pi^\pm\to e^\pm\nu_e)/\Gamma(\pi^\pm\to\mu^\pm\nu_\mu) = 1.23\times10^{-4}$ [20].

A. Particle misidentification

Misidentification of $\pi^\pm \rightleftharpoons e^\pm$ arises from E/p measurements. The misidentification probabilities are measured using samples of $K_{3\pi}$ ($\pi^\pm\to e^\pm$) and $K^+\to\pi^+\pi^0$ followed by $\pi^0\to e^+e^-\gamma$ ($e^\pm\to\pi^\pm$) decays, collected with the minimum bias trigger. In each sample, the measured contamination from other K^+ decays is below 10^{-4}. The misidentification probabilities are momentum dependent with values $P(\pi^\pm\to e^\pm) = (4-5)\times10^{-3}$ and $P(e^\pm\to\pi^\pm) = (1-3)\times10^{-2}$.

Misidentification of $\pi^\pm$ as $\mu^\pm$ arises from accidental matching of tracks with MUV3 signals or pion-induced showers in hadron calorimeters producing muons. Accidental MUV3 signals are simulated using rates measured in time sidebands within 45–75 ns of the trigger time, and hadronic showers are simulated using GEANT4. The misidentification probability is position and momentum dependent, with values of $P(\pi^\pm\to\mu^\pm) = (2-3)\times10^{-3}$.

Misidentification of $\mu^\pm$ as $\pi^\pm$ occurs due to inefficiency of the MUV3 detector. This inefficiency is measured to be 1.5×10^{-3} using kinematically selected $K^+\to\mu^+\nu_\mu$ decays from minimum-bias data, and beam halo muons.

The misidentification of $e^\pm$ as $\mu^\pm$, with probability $P(e^\pm\to\mu^\pm) = \mathcal{O}(10^{-8})$, occurs when an $e^\pm$ is absorbed or scattered inelastically upstream of the LKr. In this case no LKr energy deposit is recorded, and the track is matched with an accidental signal in MUV3. The misidentification probability is measured from data using a sample of MUV3 signals in time sidebands and depends on track momentum and extrapolated track position at MUV3.

TABLE II: Predicted backgrounds and observed numbers of events in control regions CR1 and CR2.

	$K^+\to\pi^-\mu^+e^+$		$K^+\to\pi^+\mu^-e^+$	
	CR1	CR2	CR1	CR2
Predicted	1.68 ± 0.20	1.66 ± 0.26	3.41 ± 0.54	1.27 ± 0.40
Observed	2	4	2	0

TABLE III: Predicted numbers of background events in signal regions. Decays upstream of the FV are the primary component of the $K^+\to\pi^+\pi^+\pi^-$ background.

Source	$K^+\to\pi^-\mu^+e^+$	$K^+\to\pi^+\mu^-e^+$	$\pi^0\to\mu^-e^+$
$K^+\to\pi^+\pi^+\pi^-$	0.22 ± 0.15	0.84 ± 0.34	0.22 ± 0.15
$K^+\to\pi^+e^+e^-$	0.63 ± 0.13	negligible	negligible
$K^+\to\mu^+\nu_\mu e^+e^-$	0.13 ± 0.02	negligible	negligible
$K^+\to\pi^+\pi^-e^+\nu_e$	0.07 ± 0.02	0.05 ± 0.03	0.01 ± 0.01
$K^+\to\pi^+\mu^+\mu^-$	0.01 ± 0.01	0.02 ± 0.01	negligible
$K^+\to e^+\nu_e\mu^+\mu^-$	0.01 ± 0.01	0.01 ± 0.01	negligible
Total	1.07 ± 0.20	0.92 ± 0.34	0.23 ± 0.15

B. Background evaluation

Simulations that include data-driven corrections are used to predict the background. Each simulated event is assigned a weight, which accounts for misidentification probabilities and corrects for discrepancies between data and simulations in energy deposited by $\pi^\pm$ in the LKr, as well as in the beam momentum spectrum.

The number of selected data events with $m_{\pi\mu e} < 478\,{\rm MeV}/c^2$ agrees with predictions from simulations within 3% for both the π^- and μ^- channels (Figure 3). The composition of backgrounds is similar in the control regions (CR1 and CR2) and in the signal regions. After unmasking the control regions, the predicted and observed numbers of events are largely consistent (Table II). The predicted numbers of background events from each source in the signal regions are given in Table III. The main contributions to the quoted uncertainties are the limited statistics of the simulations and the accuracy of the misidentification models.

VIII. SINGLE EVENT SENSITIVITY

The single event sensitivities, $\mathcal{B}^i_{\rm SES}$, defined for each process as the branching ratio corresponding to the observation of one signal event, are computed for each data-taking period, i, as

$$\mathcal{B}^i_{\rm SES} = \frac{1}{N^i_K A_{\rm s}\varepsilon^i_{\rm s}} = \mathcal{B}(K_{3\pi})\frac{A_{\rm n}D^i_{\rm eff}}{A_{\rm s}N^i_{3\pi}D^i_{\rm MT}}\frac{\varepsilon_{\rm n}}{\varepsilon^i_{\rm s}}\,, \quad (3)$$

where $A_{\rm s}$ are the signal acceptances (computed using simulations assuming uniform phase-space density), and $\varepsilon^i_{\rm s}$ are the trigger efficiencies for signal events, which vary

TABLE IV: Summary of inputs to the single event sensitivity calculation and corresponding resulting values for each search. The signal acceptances, $A_{\rm s}$, are displayed with statistical uncertainties only; other uncertainties quoted are quadratic sums of the statistical and systematic uncertainties.

	$K^+ \to \pi^-\mu^+e^+$	$K^+ \to \pi^+\mu^-e^+$	$\pi^0 \to \mu^-e^+$
$A_{\rm s} \times 10^2$	4.90 ± 0.02	6.21 ± 0.02	3.11 ± 0.02
$\varepsilon_{\rm LKr10} \times 10^2$	97.5 ± 1.3	97.5 ± 1.3	92.9 ± 1.2
$\varepsilon_{\rm LKr20} \times 10^2$	74.1 ± 1.6	73.3 ± 1.6	45.3 ± 1.0
$\mathcal{B}_{\rm SES} \times 10^{11}$	1.82 ± 0.08	1.44 ± 0.05	13.9 ± 0.9

due to changes in trigger downscaling factors. Efficiencies for trigger components present in both normalisation and signal trigger chains cancel in Eq. (3) to 1% precision, except for the LKr10(20) components ($\varepsilon_{\rm LKr10(20)}$), which depend on the energy deposited in the LKr and are not present in the MT trigger chain. Therefore

$$\frac{\varepsilon^i_{\rm s}}{\varepsilon_{\rm n}} = \left[1-\left(1-\frac{1}{D^i_{\rm MT}}\right)\left(1-\frac{\varepsilon_{\rm LKr10}}{D^i_{\mu{\rm MT}}}\right)\left(1-\frac{\varepsilon_{\rm LKr20}}{D^i_{e{\rm MT}}}\right)\right]D^i_{\rm eff}. \quad (4)$$

A summary of inputs to the single event sensitivity calculation is given in Table IV. For the $\pi^0 \to \mu^-e^+$ search, $\mathcal{B}^i_{\rm SES}$ is divided by $\mathcal{B}(K^+ \to \pi^+\pi^0) = (20.67 \pm 0.08) \times 10^{-2}$ [20].

The quantity $\mathcal{B}_{\rm SES}$ for the full data set is given by

$$\mathcal{B}_{\rm SES} = \left[\sum_i (\mathcal{B}^i_{\rm SES})^{-1}\right]^{-1}, \quad (5)$$

and results are shown in Table IV. The uncertainty in $\mathcal{B}_{\rm SES}$ includes the external error from the branching fractions $\mathcal{B}(K_{3\pi})$ and $\mathcal{B}(K^+ \to \pi^+\pi^0)$, each 0.4% in relative terms, and search-specific systematic uncertainties ($2\% - 7\%$) of $\mathcal{B}_{\rm SES}$, assigned to account for the precision of the data-driven corrections applied in simulations. For the LF violating $K^+ \to \pi^+\mu^+e^-$ decay $\mathcal{B}_{\rm SES} = (1.46 \pm 0.06) \times 10^{-11}$ and for the $\pi^0 \to \mu^+e^-$ decay $\mathcal{B}_{\rm SES} = (15.9 \pm 1.1) \times 10^{-11}$. Neither of these sensitivities are competitive with previous searches [13, 15].

IX. RESULTS

After unmasking the signal regions, the mass spectra for the $K^+ \to \pi^-\mu^+e^+$ and $K^+ \to \pi^+\mu^-e^+$ searches are shown in Figure 3. The numbers of predicted backgrounds ($n_{\rm bg}$) and observed events ($n_{\rm obs}$) in the signal regions are listed below

$$\begin{aligned} K^+ \to \pi^-\mu^+e^+ &: \quad n_{\rm bg} = 1.07 \pm 0.20\,, \quad n_{\rm obs} = 0; \\ K^+ \to \pi^+\mu^-e^+ &: \quad n_{\rm bg} = 0.92 \pm 0.34\,, \quad n_{\rm obs} = 2; \\ \pi^0 \to \mu^-e^+ &: \quad n_{\rm bg} = 0.23 \pm 0.15\,, \quad n_{\rm obs} = 0. \end{aligned}$$

The observations are consistent with the background predictions, and upper limits are set for the branching ratios using the $\rm CL_S$ method [21] with a likelihood ratio test statistic. The upper limits obtained at 90% CL are

$$\begin{aligned} \mathcal{B}(K^+ \to \pi^-\mu^+e^+) &< 4.2 \times 10^{-11}; \\ \mathcal{B}(K^+ \to \pi^+\mu^-e^+) &< 6.6 \times 10^{-11}; \\ \mathcal{B}(\pi^0 \to \mu^-e^+) &< 3.2 \times 10^{-10}. \end{aligned}$$

X. CONCLUSIONS

Searches for the LN violating $K^+ \to \pi^-\mu^+e^+$, and LF violating $K^+ \to \pi^+\mu^-e^+$ and $\pi^0 \to \mu^-e^+$ decays are reported. No evidence for these decays is found and upper limits are established at 90% confidence level: $\mathcal{B}(K^+ \to \pi^-\mu^+e^+) < 4.2 \times 10^{-11}$, $\mathcal{B}(K^+ \to \pi^+\mu^-e^+) < 6.6 \times 10^{-11}$, and $\mathcal{B}(\pi^0 \to \mu^-e^+) < 3.2 \times 10^{-10}$. These results improve on previous searches [12] by one order of magnitude. NA62 resumes data-taking in 2021, with the primary objective of improving the precision of the study of the $K^+ \to \pi^+\nu\bar{\nu}$ decay [18], but also with the possibility of collecting additional data to study LN and LF violating decays.

ACKNOWLEDGMENTS

It is a pleasure to express our appreciation to the staff of the CERN laboratory and the technical staff of the participating laboratories and universities for their efforts in the operation of the experiment and data processing.

The cost of the experiment and its auxiliary systems was supported by the funding agencies of the Collaboration Institutes. We are particularly indebted to: F.R.S.-FNRS (Fonds de la Recherche Scientifique - FNRS), Belgium; NSERC (Natural Sciences and Engineering Research Council), funding SAPPJ-2018-0017 Canada; MEYS (Ministry of Education, Youth and Sports), Czech Republic; BMBF (Bundesministerium für Bildung und Forschung) contracts 05H12UM5, 05H15UMCNA and 05H18UMCNA, Germany; INFN (Istituto Nazionale di Fisica Nucleare), Italy; MIUR (Ministero dell'Istruzione, dell'Università e della Ricerca), Italy; CONACyT (Consejo Nacional de Ciencia y Tecnología), Mexico; IFA (Institute of Atomic Physics) Romanian CERN-RO No.1/16.03.2016 and Nucleus Programme PN 19 06 01 04, Romania; INR-RAS (Institute for Nuclear Research of the Russian Academy of Sciences), Moscow, Russia; JINR (Joint Institute for Nuclear Research), Dubna, Russia; NRC (National Research Center) "Kurchatov Institute" and MESRF (Ministry of Education and Science of the Russian Federation), Russia; MESRS (Ministry of Education, Science, Research and Sport), Slovakia; CERN (European Organization for Nuclear Research), Switzerland; STFC (Science and Technology Facilities Council), United Kingdom; NSF (National Science Foundation) Award Numbers 1506088 and 1806430,

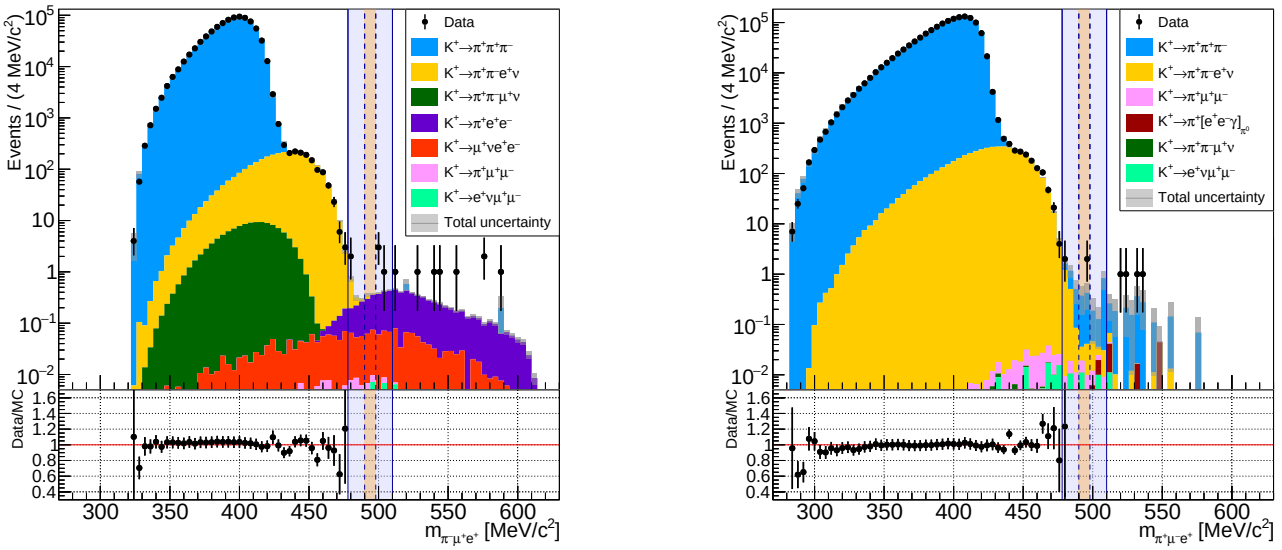

FIG. 3: Reconstructed $m_{\pi\mu e}$ spectra for selected events in searches for $K^+ \to \pi^-\mu^+e^+$ (left) and $K^+ \to \pi^+\mu^-e^+$ (right) for data (black markers) and simulated background (filled areas) samples. Ratios between the observed numbers of data events and the predicted numbers of events from MC simulations are shown in the lower panels.

U.S.A.; ERC (European Research Council) "UniversaLepto" advanced grant 268062, "KaonLepton" starting grant 336581, Europe.

Individuals have received support from: Charles University Research Center (UNCE/SCI/013), Czech Republic; Ministero dell'Istruzione, dell'Università e della Ricerca (MIUR "Futuro in ricerca 2012" grant RBFR12JF2Z, Project GAP), Italy; Russian Science Foundation (RSF 19-72-10096), Russia; the Royal Society (grants UF100308, UF0758946), United Kingdom; STFC (Rutherford fellowships ST/J00412X/1, ST/M005798/1), United Kingdom; ERC (grants 268062, 336581 and starting grant 802836 "AxScale"); EU Horizon 2020 (Marie Skłodowska-Curie grants 701386, 754496, 842407, 893101).

[1] R. Aaij *et al.*, arXiv:2103.11769.
[2] P. Minkowski, Phys. Lett. B **67**, 421 (1977).
[3] J. Pati and A. Salam, Phys. Rev. D **10**, 27 (1974).
[4] M. Bordone *et al.*, J. High Energy Phys. **10**, 148 (2018).
[5] L.G. Landsberg, Phys. Atom. Nucl. **68**, 1190 (2005).
[6] P. Langacker, Rev. Mod. Phys. **81**, 1199 (2009).
[7] C. Cornella, P. Paradisi, and O. Sumensari, J. High Energy Phys. **01**, 158 (2020).
[8] R. Aaij *et al.*, Phys. Rev. Lett. **123**, 241802 (2019).
[9] A. Baldini *et al.*, Eur. Phys. J. C **76**, 434 (2016).
[10] L. Littenberg and R. Shrock, Phys. Lett. B **491**, 285 (2000).
[11] E. Cortina Gil *et al.*, Phys. Lett. B **797**, 134794 (2019).
[12] R. Appel *et al.*, Phys. Rev. Lett. **85**, 2877 (2000).
[13] A. Sher *et al.*, Phys. Rev. D **72**, 012005 (2005).
[14] R. Appel *et al.*, Phys. Rev. Lett **85**, 2450 (2000).
[15] E. Abouzaid *et al.*, Phys. Rev. Lett. **100**, 131803 (2008).
[16] E. Cortina Gil *et al.*, JINST **12**, P05025 (2017).
[17] R. Ammendola *et al.*, Nucl. Instrum. Meth. **A929**, 1 (2019).
[18] E. Cortina Gil *et al.*, arXiv:2103.15389.
[19] J. Allison *et al.*, Nucl. Instrum. Meth. **A835**, 186 (2016).
[20] P. Zyla *et al.*, Prog. Theor. Exp. Phys. **2020**, 083C01 (2020).
[21] A. Read, J. Phys. G **28**, 2693 (2002).

NA62 Collaboration

R. Aliberti[5, a], F. Ambrosino[11], R. Ammendola[19], B. Angelucci[31], A. Antonelli[10], G. Anzivino[12], R. Arcidiacono[20, b], T. Bache[29], A. Baeva[24], D. Baigarashev[24], M. Barbanera[13], J. Bernhard[28], A. Biagioni[18], L. Bician[27, c], C. Biino[21], A. Bizzeti[8, d], T. Blazek[27], B. Bloch-Devaux[20], V. Bonaiuto[19, e], M. Boretto[20, c], A. M. Bragadireanu[23], D. Britton[31], F. Brizioli[12], M. B. Brunetti[29, f], D. Bryman[3, g], F. Bucci[8], T. Capussela[11], J. Carmignani[33], A. Ceccucci[28], P. Cenci[13], V. Cerny[27], C. Cerri[16], B. Checcucci[13], A. Conovaloff[34], P. Cooper[34], E. Cortina Gil[1], M. Corvino[11, c], F. Costantini[14], A. Cotta Ramusino[6], D. Coward[34, h], G. D'Agostini[17], J. B. Dainton[33], P. Dalpiaz[7], H. Danielsson[28], N. De Simone[28, i], D. Di Filippo[11], L. Di Lella[14, j], N. Doble[14, j], V. Duk[29, k], F. Duval[28], B. Döbrich[28], D. Emelyanov[24], J. Engelfried[22], T. Enik[24], N. Estrada-Tristan[22, l], V. Falaleev[24], R. Fantechi[16], V. Fascianelli[29, m], L. Federici[28], S. Fedotov[25], A. Filippi[21], M. Fiorini[7], J. R. Fry[29],

J. Fu[3], A. Fucci[19], L. Fulton[32], E. Gamberini[28, n], G. Georgiev[10, o], S. A. Ghinescu[23], A. Gianoli[6], M. Giorgi[14], S. Giudici[14], F. Gonnella[29], E. Goudzovski[29], C. Graham[31], R. Guida[28], E. Gushchin[25], F. Hahn[28, †], H. Heath[30], J. Henshaw[29], E. B. Holzer[28], T. Husek[4, p], O. E. Hutanu[23], D. Hutchcroft[32], L. Iacobuzio[29], E. Iacopini[9], E. Imbergamo[12], B. Jenninger[28], J. Jerhot[4, q], R. W. L. Jones[33], K. Kampf[4], V. Kekelidze[24], S. Kholodenko[26], G. Khoriauli[5, r], A. Khotyantsev[25], A. Kleimenova[1], A. Korotkova[24], M. Koval[28, s], V. Kozhuharov[10, o], Z. Kucerova[27], Y. Kudenko[25, t], J. Kunze[5], V. Kurochka[25], V. Kurshetsov[26], G. Lamanna[14], G. Lanfranchi[10], E. Lari[14], G. Latino[9], P. Laycock[28, u], C. Lazzeroni[29], G. Lehmann Miotto[28], M. Lenti[9], E. Leonardi[18], P. Lichard[28], L. Litov[24, o], R. Lollini[12], D. Lomidze[5, v], A. Lonardo[18], P. Lubrano[13], M. Lupi[13, w], N. Lurkin[29, q], D. Madigozhin[24], I. Mannelli[15], A. Mapelli[28], F. Marchetto[21], R. Marchevski[28, x], S. Martellotti[10], P. Massarotti[11], K. Massri[28], E. Maurice[32, y], M. Medvedeva[25], A. Mefodev[25], E. Menichetti[20], E. Migliore[20], E. Minucci[1, c, z, *], M. Mirra[11], M. Misheva[24, aa], N. Molokanova[24], M. Moulson[10], S. Movchan[24], M. Napolitano[11], I. Neri[7], F. Newson[29], A. Norton[7, ab], M. Noy[28], T. Numao[2], V. Obraztsov[26], A. Ostankov[26, †], S. Padolski[1, u], R. Page[30], V. Palladino[28, ac], A. Parenti[9], C. Parkinson[29, q], E. Pedreschi[14], M. Pepe[13], M. Perrin-Terrin[28, ad, ae], L. Peruzzo[5], P. Petrov[1], Y. Petrov[2], F. Petrucci[7], R. Piandani[12, af], M. Piccini[13], J. Pinzino[28, ag], I. Polenkevich[24], L. Pontisso[16], Yu. Potrebenikov[24], D. Protopopescu[31], M. Raggi[17], A. Romano[29], P. Rubin[34], G. Ruggiero[33, x], V. Ryjov[28], A. Salamon[19], C. Santoni[12], G. Saracino[11], F. Sargeni[19, ah], S. Schuchmann[28, j], V. Semenov[26, †], A. Sergi[29, ai], A. Shaikhiev[1, aj], S. Shkarovskiy[24], D. Soldi[20], M. Sozzi[14], T. Spadaro[10], F. Spinella[16], A. Sturgess[29], V. Sugonyaev[26], J. Swallow[29, *], S. Trilov[30], P. Valente[18], B. Velghe[2], S. Venditti[28], P. Vicini[18], R. Volpe[1, ak], M. Vormstein[5], H. Wahl[7, j], R. Wanke[5], B. Wrona[32], O. Yushchenko[26], M. Zamkovsky[4], A. Zinchenko[24, †]

[1]Université Catholique de Louvain, B-1348 Louvain-La-Neuve, Belgium
[2]TRIUMF, Vancouver, British Columbia, V6T 2A3, Canada
[3]University of British Columbia, Vancouver, British Columbia, V6T 1Z4, Canada
[4]Charles University, 116 36 Prague 1, Czech Republic
[5]Institut für Physik and PRISMA Cluster of Excellence, Universität Mainz, D-55099 Mainz, Germany
[6]INFN, Sezione di Ferrara, I-44122 Ferrara, Italy
[7]Dipartimento di Fisica e Scienze della Terra dell'Università e INFN, Sezione di Ferrara, I-44122 Ferrara, Italy
[8]INFN, Sezione di Firenze, I-50019 Sesto Fiorentino, Italy
[9]Dipartimento di Fisica e Astronomia dell'Università e INFN, Sezione di Firenze, I-50019 Sesto Fiorentino, Italy
[10]Laboratori Nazionali di Frascati, I-00044 Frascati, Italy
[11]Dipartimento di Fisica "Ettore Pancini" e INFN, Sezione di Napoli, I-80126 Napoli, Italy
[12]Dipartimento di Fisica e Geologia dell'Università e INFN, Sezione di Perugia, I-06100 Perugia, Italy
[13]INFN, Sezione di Perugia, I-06100 Perugia, Italy
[14]Dipartimento di Fisica dell'Università e INFN, Sezione di Pisa, I-56100 Pisa, Italy
[15]Scuola Normale Superiore e INFN, Sezione di Pisa, I-56100 Pisa, Italy
[16]INFN, Sezione di Pisa, I-56100 Pisa, Italy
[17]Dipartimento di Fisica, Sapienza Università di Roma e INFN, Sezione di Roma I, I-00185 Roma, Italy
[18]INFN, Sezione di Roma I, I-00185 Roma, Italy
[19]INFN, Sezione di Roma Tor Vergata, I-00133 Roma, Italy
[20]Dipartimento di Fisica dell'Università e INFN, Sezione di Torino, I-10125 Torino, Italy
[21]INFN, Sezione di Torino, I-10125 Torino, Italy
[22]Instituto de Física, Universidad Autónoma de San Luis Potosí, 78240 San Luis Potosí, Mexico
[23]Horia Hulubei National Institute of Physics for R&D in Physics and Nuclear Engineering, 077125 Bucharest-Magurele, Romania
[24]Joint Institute for Nuclear Research, 141980 Dubna (MO), Russia
[25]Institute for Nuclear Research of the Russian Academy of Sciences, 117312 Moscow, Russia
[26]Institute for High Energy Physics - State Research Center of Russian Federation, 142281 Protvino (MO), Russia
[27]Faculty of Mathematics, Physics and Informatics, Comenius University, 842 48, Bratislava, Slovakia
[28]CERN, European Organization for Nuclear Research, CH-1211 Geneva 23, Switzerland
[29]University of Birmingham, Edgbaston, Birmingham, B15 2TT, UK
[30]University of Bristol, Bristol, BS8 1TH, UK
[31]University of Glasgow, Glasgow, G12 8QQ, UK
[32]University of Liverpool, Liverpool, L69 7ZE, UK
[33]University of Lancaster, Lancaster, LA1 4YW, UK
[34]George Mason University, Fairfax, VA 22030, USA

[*]elisa.minucci@cern.ch, joel.christopher.swallow@cern.ch
[†]Deceased

[a]Present address: Institut für Kernphysik and Helmholtz Institute Mainz, Universität Mainz, Mainz, D-55099, Germany
[b]Also at Università degli Studi del Piemonte Orientale, I-13100 Vercelli, Italy
[c]Present address: CERN, European Organization for Nuclear Research, CH-1211 Geneva 23, Switzerland
[d]Also at Dipartimento di Fisica, Università di Modena e Reggio Emilia, I-41125 Modena, Italy
[e]Also at Department of Industrial Engineering, University of Roma Tor Vergata, I-00173 Roma, Italy
[f]Present address: Department of Physics, University of Warwick, Coventry, CV4 7AL, UK
[g]Also at TRIUMF, Vancouver, British Columbia, V6T 2A3, Canada
[h]Also at SLAC National Accelerator Laboratory, Stanford University, Menlo Park, CA 94025, USA
[i]Present address: DESY, D-15738 Zeuthen, Germany
[j]Present address: Institut für Physik and PRISMA Cluster of Excellence, Universität Mainz, D-55099 Mainz, Germany
[k]Present address: INFN, Sezione di Perugia, I-06100 Perugia, Italy
[l]Also at Universidad de Guanajuato, 36000 Guanajuato, Mexico
[m]Present address: Center for theoretical neuroscience, Columbia University, New York, NY 10027, USA
[n]Present address: University of Lancaster, Lancaster, LA1 4YW, UK
[o]Also at Faculty of Physics, University of Sofia, BG-1164 Sofia, Bulgaria
[p]Present address: Department of Astronomy and Theoretical Physics, Lund University, Lund, SE 223-62, Sweden
[q]Present address: Université Catholique de Louvain, B-1348 Louvain-La-Neuve, Belgium
[r]Present address: Universität Würzburg, D-97070 Würzburg, Germany
[s]Present address: Charles University, 116 36 Prague 1, Czech Republic
[t]Also at National Research Nuclear University (MEPhI), 115409 Moscow and Moscow Institute of Physics and Technology, 141701 Moscow region, Moscow, Russia
[u]Present address: Brookhaven National Laboratory, Upton, NY 11973, USA
[v]Present address: European XFEL GmbH, D-22761 Hamburg, Germany
[w]Present address: Institut am Fachbereich Informatik und Mathematik, Goethe Universität, D-60323 Frankfurt am Main, Germany
[x]Present address: Dipartimento di Fisica e Astronomia dell'Università e INFN, Sezione di Firenze, I-50019 Sesto Fiorentino, Italy
[y]Present address: Laboratoire Leprince Ringuet, F-91120 Palaiseau, France
[z]Also at Laboratori Nazionali di Frascati, I-00044 Frascati, Italy
[aa]Present address: Institute of Nuclear Research and Nuclear Energy of Bulgarian Academy of Science (INRNE-BAS), BG-1784 Sofia, Bulgaria
[ab]Present address: University of Glasgow, Glasgow, G12 8QQ, UK
[ac]Present address: Physics Department, Imperial College London, London, SW7 2BW, UK
[ad]Present address: Aix Marseille University, CNRS/IN2P3, CPPM, F-13288, Marseille, France
[ae]Also at Université Catholique de Louvain, B-1348 Louvain-La-Neuve, Belgium
[af]Present address: University of Chinese Academy of Sciences, Beijing, 100049, China
[ag]Present address: INFN, Sezione di Pisa, I-56100 Pisa, Italy
[ah]Also at Department of Electronic Engineering, University of Roma Tor Vergata, I-00173 Roma, Italy
[ai]Present address: Dipartimento di Fisica dell'Università e INFN, Sezione di Genova, I-16146 Genova, Italy
[aj]Also at Institute for Nuclear Research of the Russian Academy of Sciences, 117312 Moscow, Russia
[ak]Present address: Faculty of Mathematics, Physics and Informatics, Comenius University, 842 48, Bratislava, Slovakia